THE JOURNAL OF BIOLOGICAL CHEMISTRY VOL. 281, NO. 50, pp. 38918–38929, December 15, 2006

Crystal Structure of the Human AAA$^+$ Protein RuvBL1*

Received for publication, June 12, 2006, and in revised form, October 18, 2006 Published, JBC Papers in Press, October 23, 2006, DOI 10.1074/jbc.M605625200

Pedro M. Matias[‡1], **Sabine Gorynia**[‡§1], **Peter Donner**[§], **and Maria Arménia Carrondo**[‡2]

From the [‡]*Instituto de Tecnologia Química e Biológica, Universidade Nova de Lisboa, Apartado 127, 2781-901 Oeiras, Portugal and* [§]*Proteinchemistry/Research Laboratories, Schering AG, 13342 Berlin, Germany*

RuvBL1 is an evolutionarily highly conserved eukaryotic protein belonging to the AAA$^+$-family of ATPases (ATPase associated with diverse cellular activities). It plays important roles in essential signaling pathways such as the c-Myc and Wnt pathways in chromatin remodeling, transcriptional and developmental regulation, and DNA repair and apoptosis. Herein we present the three-dimensional structure of the selenomethionine variant of human RuvBL1 refined using diffraction data to 2.2 Å of resolution. The crystal structure of the hexamer is formed of ADP-bound RuvBL1 monomers. The monomers contain three domains, of which the first and the third are involved in ATP binding and hydrolysis. Although it has been shown that ATPase activity of RuvBL1 is needed for several *in vivo* functions, we could only detect a marginal activity with the purified protein. Structural homology and DNA binding studies demonstrate that the second domain, which is unique among AAA$^+$ proteins and not present in the bacterial homolog RuvB, is a novel DNA/RNA-binding domain. We were able to demonstrate that RuvBL1 interacted with single-stranded DNA/RNA and double-stranded DNA. The structure of the RuvBL1·ADP complex, combined with our biochemical results, suggest that although RuvBL1 has all the structural characteristics of a molecular motor, even of an ATP-driven helicase, one or more as yet undetermined cofactors are needed for its enzymatic activity.

RuvBL1 is a ubiquitously expressed protein (1) that plays important roles in chromatin remodeling, transcription, DNA repair, and apoptosis (2, 3). The significant evolutionary conservation of RuvBL1 from yeast to man strongly suggests that it mediates important cellular functions. RuvBL1 was originally identified by several unrelated approaches and is also known as TIP49a[3] (TATA-binding protein-interacting protein) (1, 4), Rvb1p (5), TAP54α (TIP60-associated protein) (3), and Pontin52 (1). The RuvBL1 gene is essential for viability in the yeast *Saccharomyces cerevisiae* (6), *Drosophila melanogaster* (7), and in *Caenorhabditis elegans.*[4] A number of chromatin-remodeling complexes contain RuvBL1, like INO80 in yeast and human (8), which is involved in transcription and DNA repair (2), and p400 in animal cells (9). It was demonstrated that yeast Rvb1p is required for the catalytic activity of the INO80 chromatin-remodeling complex (8). RuvBL1 is also an essential component of the human histone acetylase/chromatin-remodeling complex TIP60 (3), which consists of at least 14 distinct subunits and displays histone acetylase activity on chromatin, ATPase, DNA helicase, and structural DNA binding activities.

Generally, chromatin-remodeling complexes regulate chromatin structure and are critical for DNA-based transactions in the cell (10, 11). Acetylation of nucleosomal histones leads to relaxation of chromatin structure, thus enabling various transcription factors to gain access to chromatin and to interact with DNA (12, 13). As part of a chromatin-remodeling complex, yeast Rvb1p regulates the transcription of more than 5% of yeast genes (5). The identification of RuvBL1 in the human RNA polymerase II holoenzyme complex (6) is an additional hint at a role in transcriptional processes.

Two major oncogenic pathways in mammalian cells critically depend on RuvBL1, one involving c-Myc and another, β-catenin. RuvBL1 interacts with c-Myc and constitutes an essential cofactor for oncogenic transformation by c-Myc (14) for c-Myc- and E2F1-dependent apoptosis (15) and for E1A-dependent oncogenic transformation (9). By binding to β-catenin, RuvBL1 regulates the Wnt signaling pathway and affects β-catenin/T-cell factor-controlled transcription (7). RuvBL1 and the TIP60 histone acetyl transferase interact with sequences in the regulatory region of the ITF-2 gene, a T-cell factor downstream target. Stable expression of an ATPase-deficient RuvBL1 mutant (D302N) blocks expression of endogenous β-catenin/T-cell factor target genes, which was linked to inhibition of histone acetylation near β-catenin target gene sequences, suggesting that RuvBL1 mediates its transcriptional effects through local chromatin modifications (16).

In addition, RuvBL1 appears to be involved in small nucleolar ribonucleoprotein particle assembly, nucleolar localization, and trafficking (17, 18). The repertoire of RuvBL1 functions was furthermore extended by observations that RuvBL1 is associated with the mitotic spindle and the centrosomes via interactions with tubulin (19). These results suggest that RuvBL1 may play an important role in mitosis.

RuvBL1 belongs to a large family of ATPases known as AAA$^+$ proteins (ATPases associated with diverse cellular activities) (20) including nucleic acid-processing enzymes, chaperones, and proteases. AAA$^+$ proteins generally form hexameric ring structures and contain conserved motifs for ATP binding and hydrolysis like the Walker A (P-loop) and Walker B box (21–23), the Arg finger, and sensor residues. All AAA$^+$ proteins

* The costs of publication of this article were defrayed in part by the payment of page charges. This article must therefore be hereby marked "*advertisement*" in accordance with 18 U.S.C. Section 1734 solely to indicate this fact.

[1] Both authors contributed equally to this work.

[2] To whom correspondence should be addressed. Tel.: 351-21-4469657; Fax: 351-21-4433644; E-mail: carrondo@itqb.unl.pt.

[3] The abbreviations used are: TIP, TATA-binding protein-interacting protein; BSA, bovine serum albumin; ss-, single-stranded; ds-, double-stranded; r.m.s., root mean square; RPA, replication protein A; AMPPNP, adenosine 5′-(β,γ-imino)triphosphate.

[4] www.wormbase.org.

TABLE 1

Data collection, phasing, and refinement statistics for RuvBL1

The highest resolution shell is shown in parenthesis. R_{free} is calculated from a random sample containing 5% of the total number of independent reflections measured. B-factors were calculated from equivalent isotropic B values, including the Translation/Libration/Screw (TLS) contribution for the protein atoms.

	RuvBL1 selenomethionine		
Data collection			
Space group	P6		
Cell dimensions (Å)			
	a = 207.2		
	c = 60.77		
Wavelength (Å)	0.9791		
Resolution (Å)	45.4-2.2 (2.32-2.20)		
R_{merge}	0.068 (0.617)		
$I/\sigma(I)$	8.1 (1.2)		
Observations (unique reflections)	612,942 (73,593)		
Completeness (%)	96.5 (80.0)		
Redundancy	8.3 (3.8)		
Estimated $B_{overall}$ (Å^2)	41.1		
Refinement			
Resolution (Å)	45.4-2.2		
No. of reflections	70,028		
R_{work}/R_{free}	0.206/0.257		
No. of atoms			
Protein	8,454		
ADP	81		
Water	158		
Average B-factors	Monomer A	Monomer B	Monomer C
Protein main chain (side chain)	47.3 (51.3)	56.1 (59.4)	64.1 (66.5)
ADP (B-factor range)	27.2 (20.9-32.6)	35.5 (31.1-37.8)	47.1 (36.2-52.5)
Water (B-factor range)		47.1 (25.0-71.6)	
r.m.s. deviations			
Bond lengths (Å)	0.014		
Bond angles (°)	1.48		

use ATP binding and/or hydrolysis to exert mechanical forces, but the details of how nucleotides trigger conformational changes within individual subunits are still not completely elucidated.

RuvBL1 is the eukaryotic homologue of the bacterial DNA-dependent ATPase and helicase RuvB (24, 25), which assembles into functional homohexameric rings and is the motor that drives branch migration of the Holliday junction in the presence of RuvA and RuvC during homologous recombination (26).

In this work we have solved and refined the three-dimensional structure of the selenomethionine variant of human RuvBL1 co-purified with ADP using diffraction data to 2.2 Å of resolution. We furthermore carried out ATPase, helicase, and nucleic acid binding assays with purified RuvBL1.

EXPERIMENTAL PROCEDURES

Protein Purification—The recombinant His-FLAG tagged RuvBL1 used for structure determination was expressed in *Escherichia coli* BL21 (DE3). This strain was used for production of both the native RuvBL1 and the selenomethionine-substituted RuvBL1. For biochemical studies we used both Hi5 insect cells and *E. coli* as hosts for protein expression after making sure by using mass spectrometry that no post-translational modifications occurred in the eukaryotic system. RuvBL1 was purified as previously described (27). To obtain the His-tagged domain II construct of RuvBL1, we cloned amino acids Leu-122 to Val-238 into the pET15b vector. The DII construct was purified with a nickel-nitrilotriacetic acid.

Crystallization—Crystals of RuvBL1 were obtained at 20 °C within 2 days by the hanging drop vapor diffusion technique. Crystallization drops were mixed from equal volumes of protein solution (15 mg/ml selenomethionine RuvBL1, 20 mM Tris·HCl, pH 8.0, 150 mM NaCl, 10% glycerol, 1 mM dithiothreitol) and reservoir solution (1.6 M sodium malonate, pH 6.0). Co-crystallization with Mg^{2+} or nonhydrolyzable ATP analogs as well as with DNA of different lengths was tried but was unsuccessful. Although RuvBL1 binds nucleic acids (see below), co-crystallization was not achieved, possibly due to the existence of a mixture of different states.

Structure Determination of RuvBL1—A crystal of selenomethionine RuvBL1 was flash-frozen under a stream of nitrogen gas at 100 K using 2.0 M sodium malonate at pH 6.0 as a cryoprotecting buffer. Diffraction data were collected at European Synchrotron Radiation Facility beamline ID14-4 using an ADSC Quantum 4 detector at a wavelength corresponding to the maximal value of f″ from the selenium atoms near the x-ray absorption K-edge and were processed to 2.2 Å of resolution with XDS (28). Final data scaling, merging, and intensity conversion to structure factor amplitudes were carried out with SCALA and TRUNCATE in the CCP4 program package (29). The crystals were hexagonal and belonged to the space group *P*6 with unit-cell parameters $a = b = 207.1$ Å and $c = 60.7$ Å, with three molecules in the asymmetric unit. A summary of the data collection statistics is listed in Table 1. The structure was solved by using the Single-Wavelength Anomalous dispersion method as previously described (27). The initial RuvBL1 model was built with O (30) and Turbo-FRODO (31). Clear density was visible in the electron density maps for an ADP molecule per monomer. The structure was refined with REFMAC (32) using weak non-crystallographic symmetry restraints between the three independent monomers and Translation/Libration/Screw (TLS) rigid body refinement (33) before restrained

refinement of atomic positions and thermal motion parameters. One rigid body was defined for each of the three domains in each independent monomer. In the final refinement, 158 water molecules, located with Arp/wArp (34), were included in the model, individual restrained B-factors were refined for all non-hydrogen atoms, and hydrogen atoms were included in calculated positions. The final values of R and R_{free} were 0.206 and 0.257, respectively. The maximum likelihood estimate of overall coordinate error was 0.15 Å. Because their electron density could not be seen, the following residues are absent from the final model: 1–8, 142–155, 248–276, and 450–456 in monomer A, 1–10, 142–154, 245–278, and 449–456 in monomer B, and 1–7, 129–230, 247–276, and 450–456 in monomer C. Also, zero occupancy was given to 26 atoms in monomer A, 48 in monomer B, and 75 in monomer C. The main refinement statistics are presented in Table 1. The structure was analyzed with PROCHECK (35), and its stereochemical quality parameters were within their respective confidence intervals. The number of protein residues outside the most favored regions for non-glycine and non-proline residues in a Ramachandran (36) φ,ϕ plot was 4 (Ala-217, Glu-218, Glu-342, Thr-401) in 349 for monomer A, 3 (Gln-34, Glu-342, and Thr-401) in 344 for monomer B, and 2 (Glu-342 and Thr-401) in 273 for monomer C. The unusual φ,ϕ conformation of Thr-401 appears to be supported by its well defined electron density in the three independent monomers. However, the remaining outliers are located in regions with relatively poor electron density. The final coordinates have been deposited with the Protein Data Bank (37) with accession code 2C9O.

ATPase Assay—The reaction mixture contained 50 mM Tris-HCl, pH 7.5, 50 mM NaCl, 2 mM $MgCl_2$, 0.1 mg/ml bovine serum albumin (BSA), 1 mM dithiothreitol, 2 mM ATP, and 0.01 μCi/μl [γ-^{33}P]ATP (Amersham Biosciences). Reactions were performed in a total volume of 20 μl in the presence of 2 μg of protein. Double-stranded plasmid DNA and single-stranded oligonucleotides were used as DNA substrates and added to a final concentration of 5 ng/μl. Reactions were incubated for 30 min at 37 °C and stopped by the addition of EDTA to 0.1 M final concentration. 1-μl aliquots were spotted onto polyethyleneimine-cellulose TLC plates (Merck) that were developed with 0.5 M LiCl and 1 M formic acid. Plates were dried and exposed on a phosphorimaging screen (Eastman Kodak Co.) overnight. Spots were visualized by phosphorimaging (Personal Molecular Imager FX, Bio-Rad). SV40 large tumor antigen helicase was used as a positive control, and the D302N mutant of RuvBL1 was used as a negative control. Molecular masses of 50 kDa (RuvBL1) and 90 kDa (SV40) were used to calculate moles of hydrolyzed ATP/mol of protein.

Nucleic Acid Binding Assay—Diverse nucleotide oligomers (60-mer, 5′-CAGGCATGCAAGCTTGGCACTGGCCGTCGTTTTACAACGTCGTGACTGGGAAAACCCTGG-3′; 56-mer, 5′-TCCCAGTCACGACGTTGTAAAACGACGGCCAGTGCCAAGCTTGCATGCCTGAAATT-3′; 51-mer, 5′-AAAAAGTCGACTCTAGAGGATCCCCGGGTACCGAGCTCGAATTCGAAAAAA-3′; 41-mer, 5′-AAAAAACAGUCACGACGUUGUAAAACGACGGCCAGAAAAUU-3′) labeled with ^{33}P were used as ssDNA/RNA substrates. To generate a dsDNA substrate, the labeled 60-mer was annealed to its complementary oligonucleotide. Binding reactions were performed in a final volume of 15 μl. Nucleic acids (1 pmol) were incubated with 10 pmol of purified protein in binding buffer (15 mM HEPES, pH 6.7, 10% glycerol, 1 mM EDTA, 500 μM ATP, 1 mM dithiothreitol, and 2 mM $MgCl_2$) for 30 min at room temperature. Hi-Density Tris borate EDTA (TBE) sample buffer (Invitrogen) was added to the reaction, and the sample was separated by a 6% PAGE with 0.5 × TBE buffer and visualized by autoradiography. BSA was used as the negative control.

DNA Helicase Assay—Diverse dsDNA substrates and a DNA/RNA hybrid were generated to test helicase activities. To this effect, the ssDNA plasmid M13mp18 was annealed with diverse complementary oligonucleotides. Not only usual dsDNA substrates were tested but also substrates mimicking intermediates of DNA repair and transcription (a DNA/RNA hybrid and looped DNA). The M13mp18 substrates were labeled with the Klenow Enzyme using [α-^{33}P]ATP. In addition a 60-mer oligonucleotide (see "Nucleic Acid Binding Assay" under "Experimental Procedures") was labeled at the 3′ end and annealed with two different complementary 57-mer oligonucleotides (5′-TTTAAACCAGGGTTTTCCCAGTCACGACGTTGTAAAACGACGGCCAGTGCCAAGCTT-3′ and 5′-TCCCAGTCACGACGTTGTAAAACGACGGCCAGTGCCAAGCTTGCATGCCTGAAATT-3′). One resulting partial duplex DNA had a 3′ overhang, and the other one a 5′ overhang. The DNA helicase assay was performed in a final volume of 20 μl. The reaction mixture, composed of purified protein and 0.1 pmol of dsDNA substrate in reaction buffer (50 mM Tris-HCl, pH 7.5, 50 mM KCl, 4 mM $MgCl_2$, 25 μg/ml BSA, 0.5 mM dithiothreitol, 1 mM ATP), was incubated at 37 °C for 30 min. The reaction was stopped by adding 5 μl of sample buffer containing 1% SDS and 50 mM EDTA. Subsequently, the sample was separated by a 10% PAGE with 1 × Tris borate EDTA buffer and visualized by autoradiography. SV40 large tumor antigen helicase was used as a positive control.

RESULTS

Structure of the RuvBL1 Monomer—The crystal structure of RuvBL1 was solved from the P6 crystal form described previously (27) with data at 2.2 Å of resolution, showing an overall hexameric molecule where each monomer appears complexed with one ADP unit. The RuvBL1 monomer has approximate dimensions of 75 × 55 × 45 Å and contains 14 α-helices, 16 β-strands, and two 3_{10}-helices (Fig. 1, *A* and *B*). These structural elements fold into three domains (*DI*, *DII*, and *DIII*; Fig. 1*B*). DI consists of amino acids 1–120 and 296–365 with DII inserted in between and contains 6 α-helices (α1–α4, α1′, α5′), 9 β-strands (β1–β5; β1′–β4′), and 2 very short 3_{10}-helices. This domain is a triangle-shaped nucleotide binding domain with a Rossmann-like $\alpha/\beta/\alpha$-fold composed of a core β-sheet consisting of five parallel β-strands with two flanking α-helices on each side (Fig. 1*B*). The loop between β1 and α2 is the conserved P-loop (Walker A motif), which functions to bind and orient the γ-phosphate of ATP for hydrolysis. In addition, the conserved Walker B motif as well as the sensor 1 and the arginine finger for the adjacent molecule in the hexamer are also present.

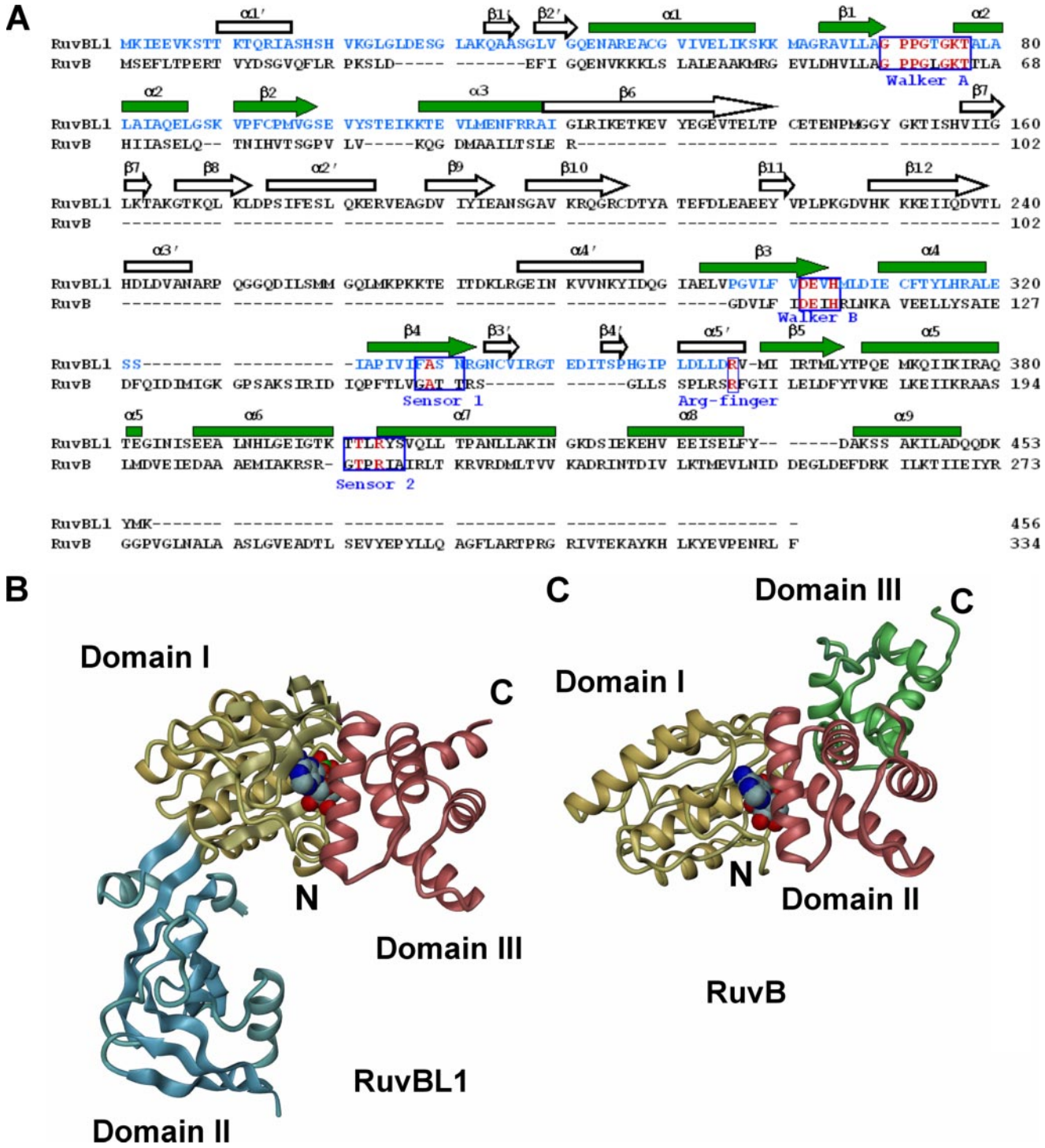

FIGURE 1. **Sequence alignment and three-dimensional structures of RuvBL1 and RuvB.** *A*, amino acid sequences of RuvBL1 and *Thermotoga maritima* RuvB were aligned by structural superposition on a three-dimensional graphics workstation. The secondary structure elements represented in *green* are common to both RuvB and RuvBL1. The numbering scheme followed was adopted to keep the numbering of secondary structure features consistent between RuvB and RuvBL1. Amino acid residues in RuvBL1 DI are represented in *light blue*. Conserved residues in the nucleotide binding motifs of both molecules are colored *red*. *B*, *ribbon diagram* of the RuvBL1 monomer showing its domain structure. The ADP molecule is depicted in a space-filling mode, where each atom is represented by a *sphere* with a diameter twice its conventional van der Waals radius. Carbon, nitrogen, oxygen, and phosphorus atoms are colored *gray*, *blue*, *red*, and *green*, respectively. *C*, *ribbon diagram* of the superposed *T. maritima* RuvB monomer (PDB 1IN7) showing its domain structure. In *B* and *C* equivalent domains in RuvBL1 and RuvB are represented in the same color. *Panels B* and *C* were prepared with DINO (A. Philippsen, personal communication).

A succinct structural comparison between the Rossmann-fold (DI) of RuvBL1 and that of other AAA$^+$ proteins is shown in Table 2. The core five-stranded β-sheet is similar to the AAA$^+$ module of other AAA$^+$ family members, such as RuvB (branch migration) (24), NSF-D2 (membrane fusion) (38), SV40 large tumor antigen and E1 protein of Papillomavirus (replication of viral DNA) (39–41), the AAA$^+$ domain of PspF (transcription activation) (42), and the hexameric ATPase P4 of

TABLE 2

Superposition of Rossmann fold (DI) in RuvBL1 with that of other AAA$^+$ proteins

The PDB files were selected from recently published structures of AAA$^+$ proteins containing ADP as ligand. However, in 1SVL and 2GXA, Mg^{2+} was also present in the ligand binding pocket, and in 1D2N the only structural data available contained ligands AMPPNP and Mg^{2+}. Rossmann folds from an arbitrarily chosen monomer in each PDB file were first superimposed using as a guide the underlined seven residues in the listed Walker A region. A least-squares fit between matching pairs of C^α atoms not more than 1.5 Å apart was then carried out.

Molecule name	PDB code	Quaternary structure in crystal	Walker A region	r.m.s. deviation C^α	Number of C^α fit in DI
RuvBL1	2C9O	Hexamer	GPPGTGKTAL		
AAA$^+$ Domain PspF	2C98	Monomer	GERGTGKELI	0.88	71
RuvB	1IN7	Monomer	GPPGTGKTTL	0.75	65
NSF-D2	1D2N	Hexamer	GPPHSGKTAL	0.95	47
SV40 Ltag helicase	1SVL	Hexamer	GPIDSGKTTL	0.97	47
E1 Papillomavirus	2GXA	Hexamer	GPPNTGKSML	1.00	42
Bϕ12 ATPase P4	1W44	Hexamer	GKGNSGKTPL	1.08	48

dsRNA bacteriophage ϕ12 (RNA packaging inside the virus capsid) (43). A striking difference, however, is that in RuvBL1 the Walker A and Walker B motifs are separated by ~170 amino acids, whereas in the other molecules they are closely spaced. The ~170-amino acid residue insertion between α3 and β3 (Fig. 1, *A* and 1*B*) constitutes the novel domain, which appears to be unique to RuvBL1 by data base searches (24). A three-dimensional structure search in the DALI server (44) revealed that the spatial arrangement of the seven β-strands (β6-β12) resembles that of the DNA binding domains of different proteins involved in DNA metabolism, such as the highly conserved eukaryotic protein replication protein A (RPA, PDB 1JMC). The DALI Z-score was 4.9, with a 2.9-Å r.m.s. deviation for the 69 superimposed C^α atoms in the ~170-residue-long RuvBL1 domain II and the 238-residue-long RPA. In the superposed regions the sequence identity was 19%. The structure of RPA (45) is composed of two domains with a similar fold, each formed by seven β-strands. A ssDNA molecule is bound to this protein and makes contacts mainly through the phosphate backbone with both domains. The presumed DNA binding region in RuvBL1 DII (residues 127–233) was superimposed with the N-terminal (residues 183–298) domain of RPA. This procedure gave r.m.s. deviation values of 0.75 Å for 33 matched C^α atoms less than 1.5 Å apart. The C^α traces of the superimposed structures are represented in Fig. 2*A*. In addition, the surface charges in the DNA binding region of RuvBL1 DII resemble those of the N-terminal domain (Fig. 2, *B* and *C*) in RPA. Our DNA binding experiments confirm that DII represents a new functional domain of eukaryotic AAA$^+$ motor proteins important for DNA/RNA binding.

The smaller third domain, DIII, is all α-helical (α5-α9). One remarkable feature of DIII is that four helices (α5-α8) form a bundle located near the "P-loop," important for ATP binding, in which α5 and the beginning of α7 covers the ATP binding pocket at the interface of DI and DIII. This domain is similar to DII in RuvB (Fig. 1, *B* and *C*). The spatial arrangement of DI, DII, and DIII in RuvBL1 could allow motions between domains.

Structure of the RuvBL1 Hexamer—RuvBL1 assembles into an hexameric structure with a central channel (Fig. 3, *A* and *B*). In the crystal structure there are three independent monomers (A, B, and C) and two crystallographically non-equivalent hexamers. One hexamer is centered on a crystallographic 6-fold axis and is formed by the 6-fold repetition of monomer A, whereas the other is centered on a crystallographic 3-fold axis and is formed by the 3-fold repetition of monomers B and C. The three independent monomers have very similar three-dimensional structures. Superposition calculations between the three monomers by least-squares fit between pairs of C^α atoms not more than 1.5 Å apart gave r.m.s. deviations between C^α atoms of 0.47 Å between monomers A and B, 0.58 Å between monomers A and C, and 0.43 Å between monomers B and C. The total number of matched pairs C^α atoms was 300, 303, and 290, respectively, and these were mostly located in DI and DIII. Domain II had a similar fold but different orientations in monomers A and B and was highly disordered in monomer C. Viewed from the top (Fig. 3*B*, with *top* and *bottom* as defined in Fig. 3*A*), the external diameter of the hexameric ring ranged between 94 and 117 Å, and the central channel had an approximate diameter of 18 Å. Also, its top surface (Fig. 3*A*) appeared to be remarkably flat. The hexamer bottom entrance was positively charged, whereas its inner surface and top entrance were negatively charged, indicating a possible function in binding and translocating single-stranded DNA (Fig. 4, *A* and *B*). DII protrudes out of the hexameric ring. The connection between the nucleic acid binding region of DII and the bulk of DI was achieved via a two-stranded extended β-region. This long connecting region probably allows DII some freedom of motion in relation to DI and DIII. Indeed, since in the RuvBL1 hexamer there are no direct contacts between the nucleic acid binding region of DII and either DI or DIII, it is very likely that the conformation and position of DII in the crystal structure was determined by crystal packing. DII of hexamer A packs between domains I and III of molecule B in hexamer BC. DII in molecule B packs against domains I and III of molecule A. However, DII in molecule C has no close crystal contacts, and this probably explains why it could not be fully seen in the electron density maps. A further indication of molecular disorder is given by the values of average thermal motion parameter B listed in Table 1; they are lowest for monomer A and highest for monomer C, consistent with the increasing number of residues (see above) that could not be seen in the electron density and, thus, were not included in the structural model. On the other hand, the B-values for the ADP ligand atoms are consistently similar to those of the protein atoms in the binding pocket. The interface between adjacent subunits in the RuvBL1 hexamer is made up entirely by DI and DIII and exhibits well defined shape complementarity. As shown in Fig. 4*C*, the hexamerization in the structure of the RuvBL1·ADP complex blocks the nucleotide binding pocket, thus making an exchange from ADP to ATP impossible. This may explain our inability to co-crystallize non-hydrolyzable ATP analogs into this crystal form (data not

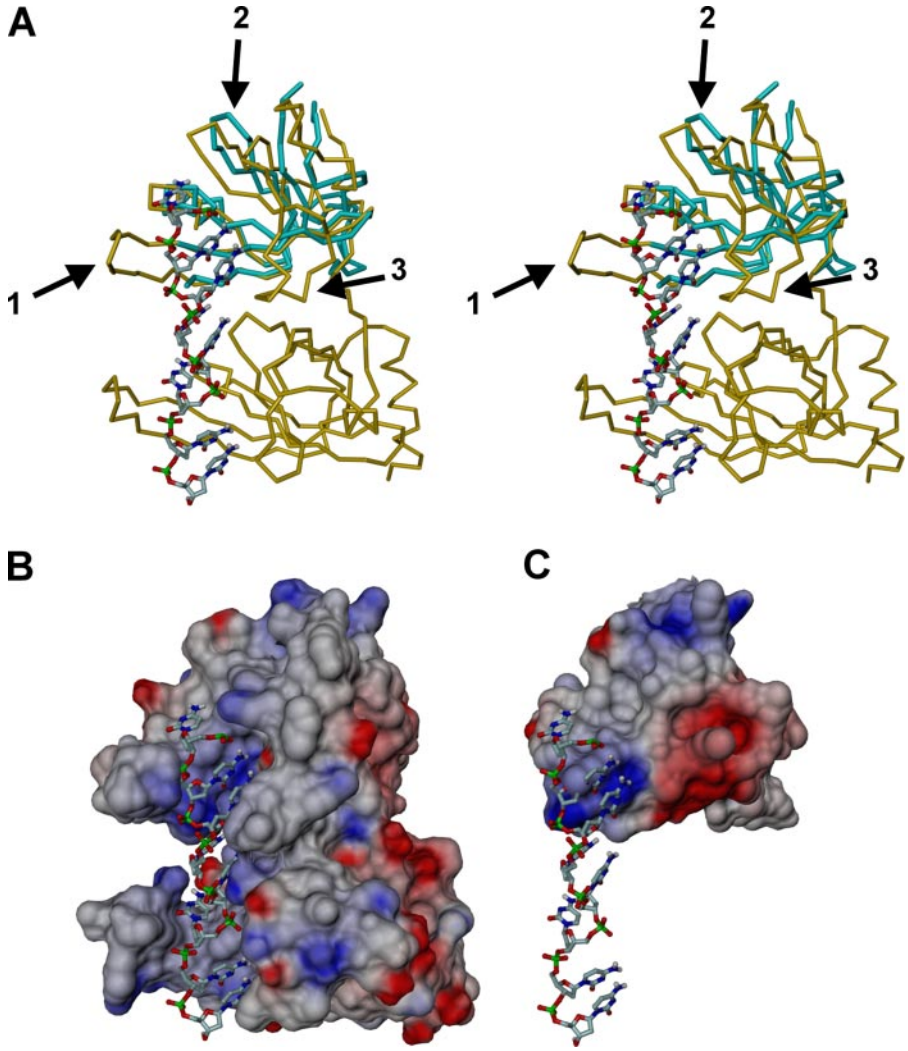

FIGURE 2. **The DNA binding region in RuvBL1 domain II.** *A*, stereoview of the protein C^{α} trace (*gold*) and ssDNA *ball-and-stick* representation (carbon, nitrogen, oxygen, and phosphorus atoms are colored *gray*, *blue*, *red*, and *green*, respectively) of the RPA molecule (PDB 1JMC) superimposed onto the DNA binding region of RuvBL1 DII (residues 127–233; *cyan*). The long loops in the N-terminal domain of RPA that interact with ssDNA (*arrows 1* and *3*) correspond to a disordered loop and a much shorter loop (*arrow 2*) in RuvBL1 DII. *B*, view of the electrostatic potential of the RPA molecule mapped at its molecular surface. The molecular surface was calculated with MSMS (65) using a probe radius of 1.4 Å, and the electrostatic potential was calculated with MEAD (66) using an ionic strength of 0.1 M, dielectric constants of 4.0 and 80.0 for the protein and the exterior, respectively, and a temperature of 300 K. The range of potentials shown spans −5 (*red*) to +5 *kT*/*e* (*blue*) units. *C*, view of the electrostatic potential of the DNA binding region of RuvBL1 DII mapped at its molecular surface. The molecular surface and the electrostatic potential were calculated as described above for the whole RuvBL1 hexamer, but for clarity only the DNA binding region of RuvBL1 DII is represented. As a visual aid, the ssDNA molecule bound to RPA is represented in *ball-and-stick* (Carbon, nitrogen, oxygen, and phosphorus atoms are colored *gray*, *blue*, *red*, and *green*, respectively). The view in *B* and *C* is the same as in Fig. 2*A*. Drawings were prepared with DINO.

shown) because these compounds would require an open conformation of the active site.

ATP Binding and Hydrolysis—Structural analysis and sequence conservation identify four motifs at the DI-DIII boundary (Walker A, Walker B, sensor 1 from DI, and sensor 2 from DIII; Figs. 1*A* and 4*D*) likely to be important in nucleotide-driven conformational changes of the protein structure. The Walker A motif, also termed the P-loop, is important for ATP binding. It coordinates the triphosphates and positions the γ-phosphate group for cleavage. The Walker A residues Gly-70 to Leu-79 in RuvBL1 have corresponding conserved residues in all structures listed in Table 3, the similarity being higher with bacterial RuvB and NSF-D2.

Using the superimposed coordinates of RuvBL1, RuvB (24), NSF-D2 (38), and SV40 large tumor antigen helicase (39, 40) together with the AMPPNP and Mg^{2+} ligands in NSF-D2, we modeled an ATP bound to RuvBL1. The nucleotide binding pocket in RuvBL1 is sufficiently large to accommodate an ATP molecule, and the γ-phosphate will occupy a volume that contains three water molecules in the ADP-bound structure (Fig. 4, *E* and *F*). Furthermore, based on the observed coordination of Mg^{2+} in NSF-D2 and SV40 large tumor antigen helicase, it is reasonable to assume that this cation could bind in an equivalent position in RuvBL1/ATP. Within the Walker A motif, Gly-73 could stabilize the γ-phosphate by interacting with one of its oxygens, and Thr-77 could be involved in coordinating the Mg^{2+} (Fig. 4*E*).

The Walker B motif residues Asp-302–His-305 are responsible for ATP hydrolysis. They lie at an adequate position to interact with Mg^{2+} and likely activate the water nucleophile for ATP cleavage. In addition to the Walker motifs, Asn-332 in sensor 1, located in DI between the Walker A and B motifs, and Arg-404 in sensor 2 make polar interactions with the β- or γ-phosphate groups. The function of sensor 1 is to distinguish between nucleotide diphosphate and triphosphate states by forming a hydrogen bond with the ATP γ-phosphate group. Based on our ATP-bound model, a simple rotamer change in response to ATP binding could bring either oxygen or nitrogen from the side chain of Asn-332 into a suitable position for hydrogen bond formation with the terminal oxygen from γ-phosphate, without a significant backbone conformational change.

The loop linking helix α6 to helix α7 protruding from DIII contains the sensor 2, which packs against the nucleotide binding site and distinguishes between nucleotide-bound and unbound states. Arg-404 in sensor 2 interacts with components of the nucleotide present in both ADP and ATP.

The conserved Arg-357 corresponds to Arg-170 in RuvB, which was shown to function as an Arg finger (24), allowing the efficient hydrolysis of ATP by binding to the γ-phosphate

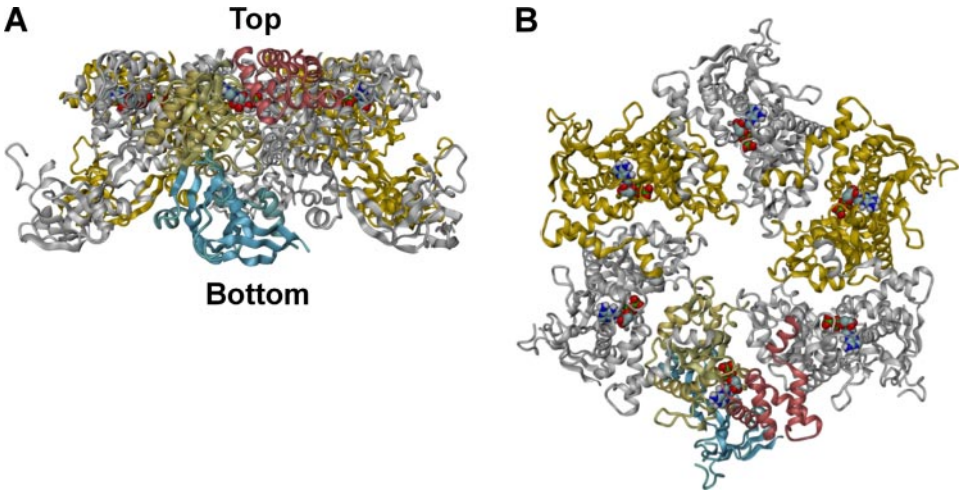

FIGURE 3. **The RuvBL1 hexamer.** *A*, *ribbon diagram* of the RuvBL1 hexamer (side view). Adjacent monomers are colored *light gray* and *gold*. One *gold* monomer is colored in the same way as in Fig. 1*B* to highlight its domain structure. The hexamer herein represented is the crystallographic hexamer, formed by monomers A around the crystallographic 6-fold axis. The bound ADP molecules are depicted in space-filling mode, where each atom is represented by a *sphere* with a diameter twice its conventional van der Waals radius. Carbon, nitrogen, oxygen, and phosphorus atoms are colored *gray*, *blue*, *red*, and *green*, respectively. *B*, *ribbon diagram* of the RuvBL1 hexamer (top view). The coloring scheme is as in *A*. Drawings were prepared with DINO.

group. In the RuvBL1 hexamer and similar to Arg-538 in the E1 protein of Papillomavirus (41), Arg-357 from the adjacent monomer contributes to the active site and is in sufficiently close proximity to the nucleotide binding pocket to be able to act as an Arg finger, provided a suitable conformational change takes place. This arrangement of active-site residues suggests some degree of cooperativity between monomers. We, therefore, propose that hexamerization is critical for ATP hydrolysis in RuvBL1; monomer assembly into hexamers is known to be crucial for the function of other AAA$^+$-class ATPases (20).

ATPase Activity of Human RuvBL1—Despite containing all the important structural motifs for ATPase activity, it was a surprising result that such activity was experimentally found to be very low in human RuvBL1. This is in contrast with the AAA$^+$ protein large tumor antigen of simian virus 40 (46), an hexameric helicase essential for viral DNA replication in eukaryotic cells (47), that was used as a positive control (Fig. 5). In addition, we observed that the ATPase activity of RuvBL1 was not stimulated by either single- or double-stranded DNA (Fig. 5) or by RNA (data not shown). The negative control RuvBL1_D302N contains a missense mutation in the Walker B motif (DEVH→NEVH), which is expected to abolish the ATPase activity of RuvBL1, and indeed exhibited no ATPase activity (Fig. 5).

In an attempt to understand the weak ATPase activity of wild-type RuvBL1, we undertook a more detailed comparison between the nucleotide binding pockets of RuvBL1 and of other AAA$^+$ proteins with known ATPase activity *in vitro*; the AAA$^+$ domain of PspF (42), RuvB (which by itself has only a low, RuvA-activated, ATPase activity) (24), NSF-D2 (whose activity is regulated by soluble NSF attachment proteins) (38), SV40 large tumor antigen (39, 40), the E1 replicative helicase from Papillomavirus (41), and the hexameric ATPase P4 of dsRNA bacteriophage ϕ12 (43). The results of this comparison are listed in Table 3 and show that RuvBL1 has the lowest solvent-accessible area among all these molecules, indicating in this case a very tightly bound ADP unit. Therefore, it cannot easily exchange with ATP, and this may be the cause for the low *in vitro* ATPase activity of RuvBL1. In addition, the adenine ring of ADP is held in place by a large number of hydrogen bonds and hydrophobic contacts, and both phosphate groups also have a large number of hydrogen bonds. The hypothesis of tight ADP binding is furthermore conveyed by the fact that helix α5 in DIII packs more closely against DI in RuvBL1 than the corresponding helix in DII against DI in either RuvB (see Fig. 6), the AAA$^+$ domain of PspF, or NSF-D2. Hexamer formation does not appear to influence ADP binding, since the capping of the nucleotide binding pocket by an adjacent monomer does not alter the solvent-accessible area calculations. However, it does obstruct a possible ADP exit channel and, thus, contributes to prevent the ADP/ATP exchange (Fig. 4*C*).

Interaction with Nucleic Acids—The diameter and the electrostatic potential of the central channel of RuvBL1 (Fig. 4, *A* and *B*) are indications that it may bind single-stranded nucleic acids. The channel diameter of about 17.7 Å (measured between C$^\beta$ atoms of Glu-342) is comparable with the 18.2-Å value determined for the hexameric replicative helicase RepA (48) (PDB 1GY8; measured between C$^\beta$ atoms of Glu-149) or the 20.7-Å value found for the hexameric ATPase P4 of dsRNA bacteriophage ϕ12 (PDB 1W44; measured between C$^\beta$ atoms of Asp-240). It is also similar to the 17.2- 18.8-Å range between C$^\beta$ atoms of His-507 and the 19.8–20.2-Å range between C$^\beta$ atoms of Lys-356, which delimit the central channel in the E1 replicative helicase from Papillomavirus (PDB 2GXA), which is occupied by a single strand of DNA (41). This diameter is in all cases too small for dsDNA to pass through. Several hexameric AAA$^+$ proteins are known to interact with nucleic acids, with the central channel of the hexamer as the most likely main interaction site, and it is believed that this interaction is mediated by one or more loops that extend into the central channel. In the case of the hexameric gene 4D ring helicase from bacteriophage T7 (T7 gp4D), three loops facing the central channel of the ring are implicated in binding to ssDNA (49). In the E1 replicative helicase from Papillomavirus (41), the ssDNA interacts via its phosphates or sugar moieties with residues from two hairpin loops, forming hydrogen bonds or van der Waals interactions. In RuvBL1, two such loops are also present; the first (residues 101–108) includes the positively charged Lys-107 and lies at the bottom of the central ring channel, whereas the second (residues 334–351) contains the negatively charged Glu-342 and is located near the top of the central ring channel (as shown in Fig. 4, *A* and *B*).

The largely negative electrostatic potential of the inner surface of the channel is similar to that in the hexameric ATPase P4

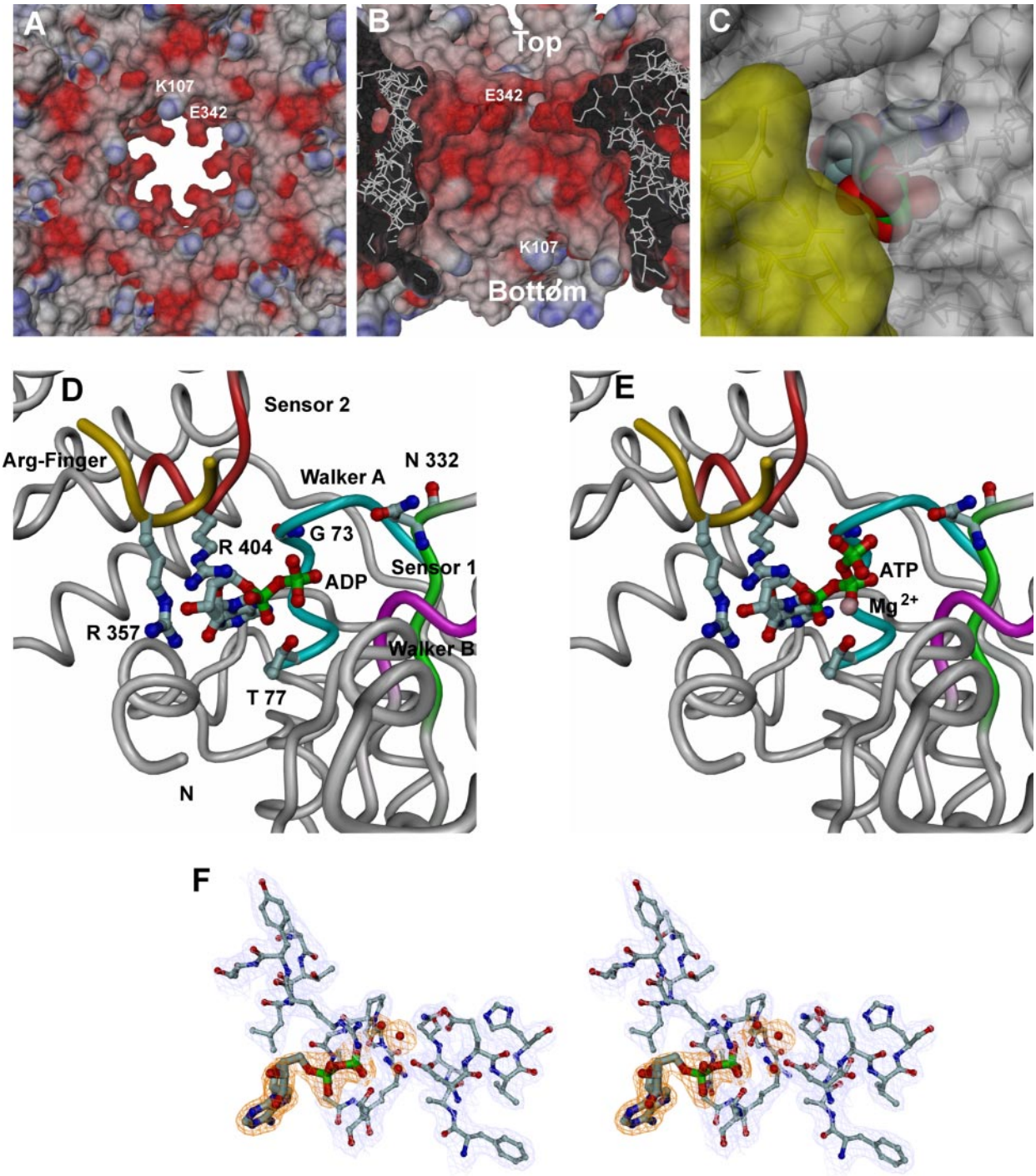

FIGURE 4. **The central hexamer channel and the nucleotide binding pocket.** *A* and *B*, views of the electrostatic potential of the RuvBL1 hexamer mapped at the molecular surface. The molecular surface and the electrostatic potentials were calculated as in Fig. 2*B* for the whole hexamer as in Fig. 2*C*. The range of potentials shown spans −5 (*red*) to +5 *kT/e* (*blue*) units. The labeled residues (Lys-107 and Glu-342) are the most conspicuous positively and negatively charged residues. Lys-107 is located near the channel bottom and Glu-342 near its top. In *A* the hexamer is shown in bottom view (as defined in Fig. 3*A*). In *B* a cross-section view of the central channel (same orientation as in Fig. 3*A*) is represented, showing a negatively charged patch that covers most of its surface. *C*, view of the interface between adjacent monomers in the RuvBL1 hexamer, showing blocking of the nucleotide binding pocket upon hexamer formation. The molecular surfaces represented (*gold* and *white*) were calculated as in Fig. 2, *B* and *C*. The ADP molecule is represented in space-filling mode, as in Fig. 1*B*. *D*, tube view of RuvBL1 in the vicinity of the nucleotide binding pocket, showing the Walker A (*cyan*), Walker B (*violet*), sensor 1 (*green*) and sensor 2 (*red*) regions as well as the Arg finger region from the adjacent monomer (*gold*). The ADP molecule and the side chains of important residues mentioned under "Results" are represented in *ball-and-stick* mode. Carbon, nitrogen, oxygen, and phosphorus atoms are colored *gray*, *blue*, *red*, and *green*, respectively. *E*, a similar view as in *D*, showing the modeled positions of ATP and Mg^{2+}. *F*, stereoview showing a composition of an $Fo - Fc$ electron density omit map (colored *orange* and drawn at the 2.5 map r.m.s. level) around the ADP molecule and its nearest water molecules together with the final 2 $Fo - Fc$ electron density map (drawn at 1.0 map r.m.s. level) around its nearest protein neighbors in Walker A, Walker B, sensor 1, and sensor 2 regions (represented in *ball-and-stick* mode). The omit map was calculated using values of Fc, and phases were obtained after 10 cycles of REFMAC refinement of the final model, after removal of all ADP and water molecules. To minimize model bias, these coordinates were applied a random shift with a maximum amplitude 0.5 Å before refinement. This refinement converged to $R = 0.246$ and $R_{free} = 0.295$. The ADP molecule is represented in *ball-and-stick* mode. Carbon, nitrogen, oxygen, and phosphorus atoms are colored *gray*, *blue*, *red*, and *green*, respectively. Drawings were prepared with DINO.

TABLE 3

Characterization of nucleotide binding pocket in RuvBL1 and other AAA$^+$ proteins

The location of the nucleotide binding pocket occurs either at the interface between two domains within a monomer (DI/DII or DI/DIII interface) or at the interface between two adjacent monomers in the hexamer (M/M interface). The solvent-accessible area was calculated with NACCESS (67), excluding the effects of water molecules present in the PDB file. Symmetry-related molecules were included where appropriate to avoid systematic errors due to incomplete protein neighbourhood of the ligand. Where there was more than one copy of the nucleotide ligand present, the lowest value of solvent-accessible area was used. The hydrogen bonds and hydrophobic contacts were calculated with LIGPLOT/HBPLUS (64, 68).

Molecule	PDB code	Location of nucleotide binding pocket	Ligand	Accessible area	Ligand hydrogen bonds with (ligand number of atoms with hydrophobic contacts to) protein/water atoms				
					Adenine	Sugar	P_α	P_β	P_γ
				Å^2					
RuvBL1	2C9O	DI/DIII interface	ADP	13.5	5 (4)	1 (1)	5	6	
AAA$^+$ Domain PspF	2C98	DI/DII interface	ADP	114.5	4 (3)	3 (1)	3	7	
RuvB	1IN7	DI/DII interface	ADP	39.4	3 (5)	0 (1)	3	7	
NSF-D2	1D2N	DI/DII interface	AMPPNP, Mg^{2+}	55.7	3 (4)	3 (0)	3	3	5
SV40 LTag helicase	1SVL	M/M interface	ADP, Mg^{2-}	37.4	2 (3)	1 (1)	3	10	
E1 Papillomavirus	2GXA	M/M interface	ADP, Mg^{2-}	67.0	0 (4)	0 (0)	4	6	
Bϕ12 ATPase P4	1W44	M/M interface	ADP	90.1	3 (5)	3 (2)	5	3	

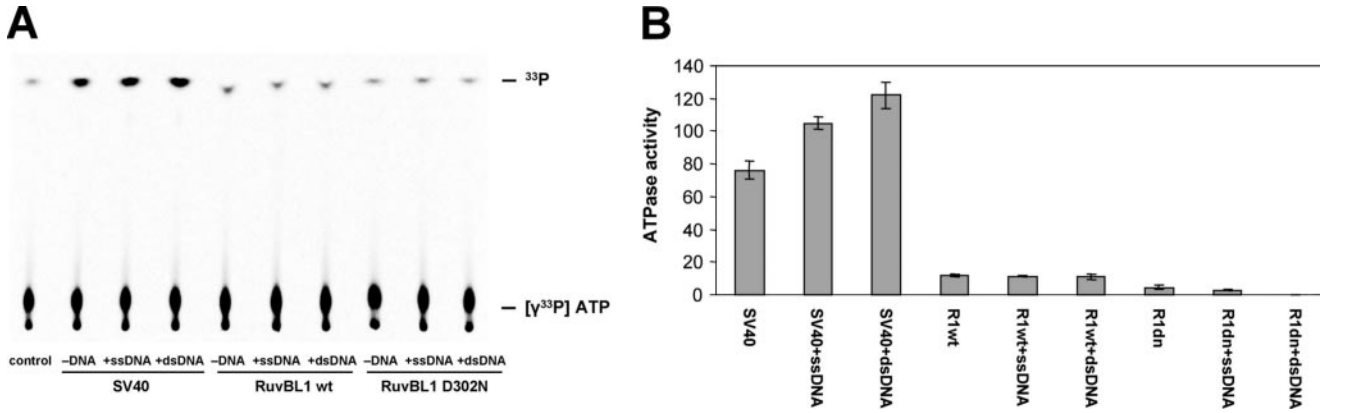

FIGURE 5. **ATPase activity of human RuvBL1.** *A*, free phosphate ^{33}P produced by hydrolysis of ATP was separated from [γ-^{33}P] ATP by thin-layer chromatography. Free phosphate (fast migrating spot) and ATP (slowly migrating spot) were visualized by autoradiography. Note that a trace amount of free phosphate contaminated ATP (control). *B*, quantification of ATPase activity. Activity is expressed as mol of ATP hydrolyzed/mol of protein.

of dsRNA bacteriophage ϕ12 (43), which binds to ssRNA, and also to that in the helicase RepA (48). In contrast, channels shown to bind to dsDNA are wider and positively charged (39, 50) to be able to accommodate the negatively charged dsDNA sugar-phosphate backbone. This is clearly the case of SV40 large tumor antigen helicase (39, 40), which has a positively charged central channel sufficiently wide to accommodate strand separation and forked DNA unwinding.

The interaction with single-stranded nucleic acid molecules in the inner channel of RuvBL1 may eventually be similar to that described for T7 gp4D (49). T7 gp4D has a preference for forked DNA substrates with two single-stranded tails of sufficient length that allow the hexamer to assemble on the DNA and begin unwinding of the duplex (51, 52). The 5′ tail of the forked DNA passes through the center of the ring (53), whereas the 3′ tail is thought to contact the outside of the ring (51). In T7 gp4D there is no obvious DNA binding surface on the outside of the ring for the 3′ tail of the forked dsDNA. In RuvBL1 however, the novel domain II is likely to represent such an interaction region.

Using an electrophoretic mobility shift assay we showed that RuvBL1 binds to ssDNA and dsDNA as well as to ssRNA (Fig. 7). Because the central channel seems to be too small to accommodate dsDNA, we surmised that a region outside of the ring makes DNA contacts. Based on this assumption and the similarity between DII and DNA binding domains of other proteins, we cloned and purified the His-tagged DII of RuvBL1 (Leu-122–Val-238) and used the pure domain in electrophoretic mobility shift assay experiments. Our results confirmed that the new domain II is a nucleic acid binding domain (Fig. 7*A*). Furthermore, we cloned RuvBL1 without DII to test whether nucleic acid binding is decreased to that mutant, but unfortunately the construct was not soluble (data not shown). Therefore, we conclude that DII is important for proper folding and the stability of RuvBL1. Because the labeled nucleic acid substrates did not bind to the BSA protein used as control, our results indicated that they were specifically bound to RuvBL1 and DII. We believe that RuvBL1 can bind to nucleic acids in a sequence-independent manner because the sequence of diverse nucleic acid substrates was chosen randomly (Fig. 7*B*).

Lack of in Vitro Helicase Activity of Purified Human RuvBL1—A 3′ to 5′ DNA helicase activity has been reported for rat RuvBL1 recombinantly expressed and purified from bacterial cells (54). However, other groups failed to detect helicase activity for recombinant human RuvBL1 (3, 6). To clarify this, we tested not only 3′ to 5′ and 5′ to 3′ dsDNA substrates but also substrates mimicking intermediates of transcription and DNA repair such as DNA/RNA hybrids and loop-forming dsDNA. However, we were unable to detect significant helicase activity using purified human RuvBL1 (Fig. 8, *A* and *B*) in agreement

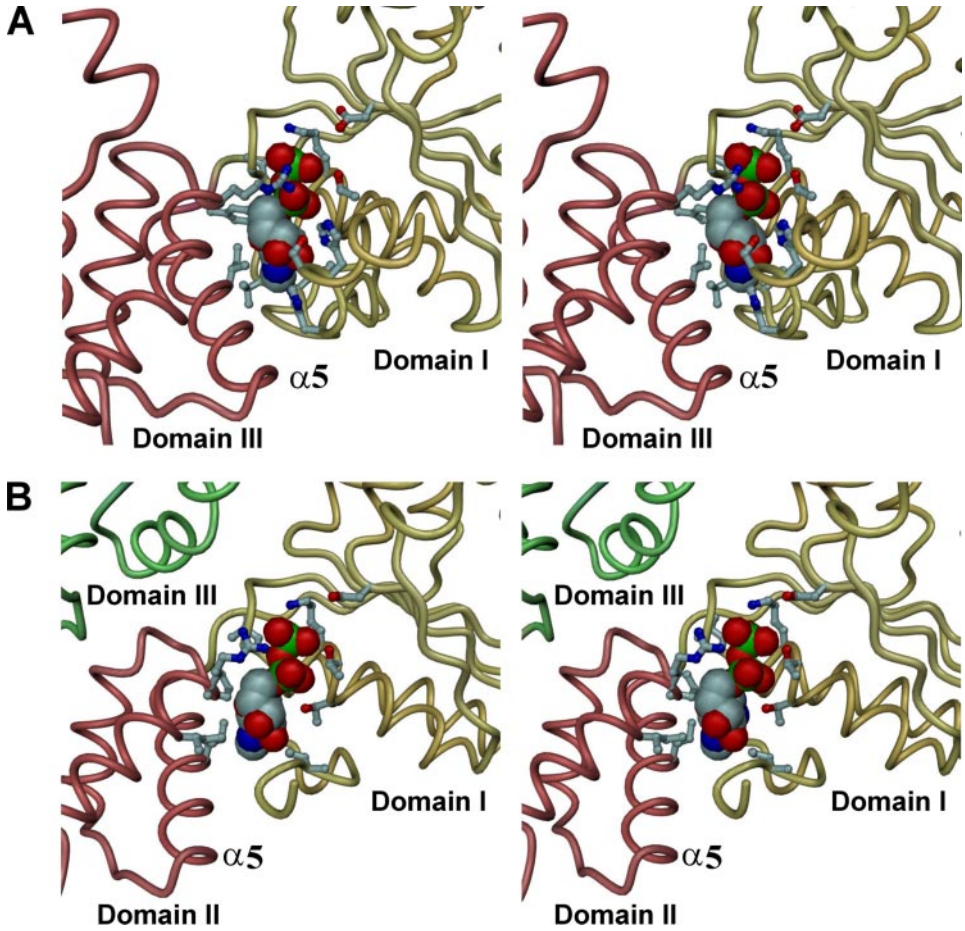

FIGURE 6. **ADP tight binding in the nucleotide binding pocket of RuvBL1.** Stereo detail views of the nucleotide binding pocket in RuvBL1 (*A*) and RuvB (*B*) structures showing the closer packing of helix α5 in DIII against DI in RuvBL1, in comparison with the packing of helix α5 in DII against DI in RuvB. The side chains of the protein residues that contribute to the hydrogen bonds and hydrophobic contacts with ADP enumerated in Table 3 are represented in *ball-and-stick* mode. Carbon, nitrogen, oxygen, and phosphorus atoms are colored *gray*, *blue*, *red*, and *green*, respectively. The protein chains are represented as tube C^{α} diagrams. Equivalent domains in RuvBL1 and RuvB are represented in the same color. The ADP molecule is depicted in a space-filling mode, where each atom is represented by a *sphere* with a diameter twice its conventional van der Waals radius. Drawings were prepared with DINO.

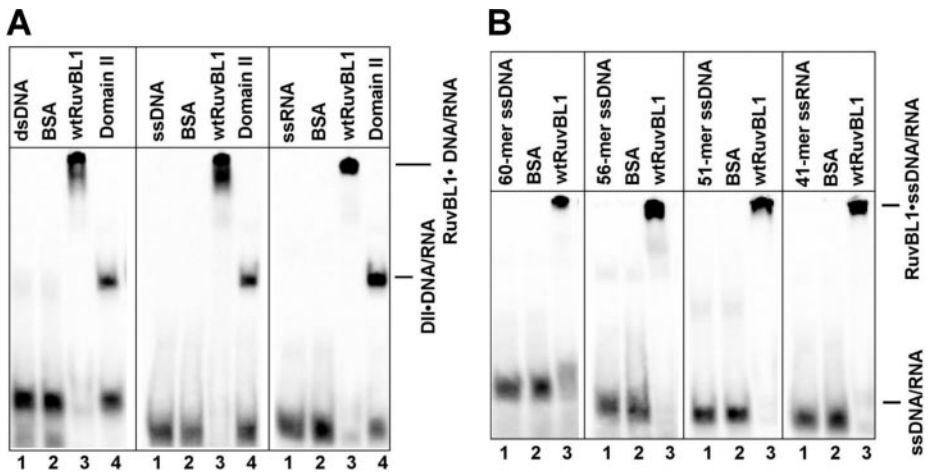

FIGURE 7. **Nucleic acid binding to human RuvBL1.** *A*, ssDNA/RNA and dsDNA binding of human RuvBL1 (*lane 3*) and domain II of RuvBL1 (*lane 4*) by electrophoretic mobility shift assay. Isolated DNA substrate was analyzed (*lane 1*) to identify the positions of ssDNA and dsDNA, respectively. The BSA control (*lane 2*) was used to ensure that dsDNA and ssDNA specifically interacted with RuvBL1. *B*, further electrophoretic mobility shift assay with three different ssDNA substrates with diverse sequences and a ssRNA substrate to confirm nucleic acid binding to RuvBL1 (*lanes 3*) in a sequence-independent fashion. The samples were analyzed on a 6% nondenaturing polyacrylamide gel and visualized by autoradiography. The shifted protein-DNA complexes are indicated in the figure.

with the previously published data (3, 6). Helicase activity in hexameric AAA^+ proteins results from a mechanical motion derived from ATP hydrolysis. One essential requirement for the continued motion driven by the hydrolysis of ATP is the rapid exchange at the active site between the hydrolysis products ADP + P_i and a new ATP molecule. In RuvBL1, hexamer formation and tight ADP binding appear to block the ADP/ATP exchange and, thus, severely lower its ATPase activity. On the other hand, hexamer formation seems to be crucial for ATP hydrolysis, because the essential residue Arg-357, which is the likeliest candidate to act as an arginine finger, is provided by an adjacent monomer. Because we have shown that nucleic acids do bind to RuvBL1 in a sequence-independent fashion, the lack of *in vitro* helicase activity for RuvBL1 is most likely a consequence of its lack of significant ATPase activity.

DISCUSSION

The three-dimensional hexameric structure presented here confirms that human RuvBL1 is an AAA^+ protein with a typical nucleotide binding domain and reveals the existence of a new domain that binds to nucleic acids. The involvement of RuvBL1 in chromatin remodeling (2, 8, 9) suggests that it can bind to dsDNA. RuvBL1 could function as a helicase during chromatin remodeling since access to the genetic information is necessary during transcription and DNA repair. It has been shown that RuvBL1 functions in that context (3, 7, 55). In this case RuvBL1 would also have to bind to ssDNA. In addition, RNA binding could be important during transcription and small nucleolar ribonucleoprotein assembly for dissolving stable tertiary RNA structures (6, 56). We have shown from our biochemical experiments that RuvBL1 binds to dsDNA, ssDNA, and ssRNA in a nonsequence-specific fashion, in line with an implication in processes

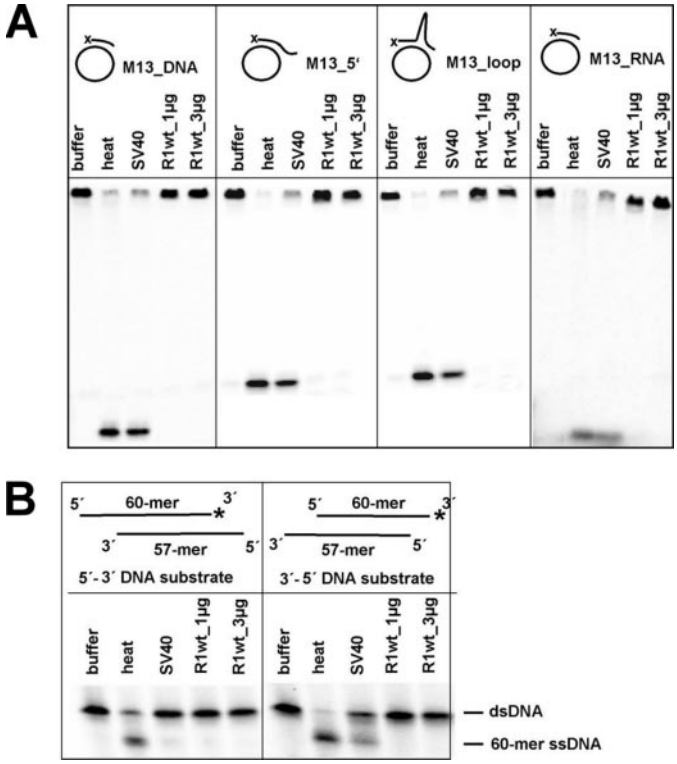

FIGURE 8. **Helicase activity of human RuvBL1.** Helicase activity assay of human RuvBL1 using diverse M13mp18 DNA substrates (*A*) and 5′ to 3′ and 3′ to 5′ substrates (*B*). An *asterisk* denotes the ^{33}P label. DNA helicase activity was tested with 2 μg of the positive control SV40 large tumor antigen helicase (*lane 3*) and 1 and 3 μg of wtRuvBL1 per reaction (*lanes 4* and *5*). A boiled probe was analyzed to identify the position of ssDNA (*lane 2*).

that require binding to nucleic acid. We believe that the protein-nucleic acid interaction is achieved via the sugar-phosphate backbone of the DNA and RNA. It is known that RuvBL1 can be recruited by diverse transcription factors, which may be important in guiding it to the correct target DNA (7, 14, 16). Although it has been shown *in vivo* that the ATPase activity of RuvBL1 is needed for several functions (5, 14, 16), we could only detect a marginal ATPase activity and were not able to detect any helicase activity for purified human RuvBL1 in agreement with the results of Ikura *et al.* (3) and Qiu *et al.* (6). Important cellular processes such as those dealing with DNA metabolism are often regulated by large multiprotein complexes, and it is, therefore, likely that full RuvBL1 enzymatic activity can only be seen in such an environment. It is for instance known that many hexameric helicases interact with accessory proteins (57–60). Conversely, viral genomes are much smaller and helicases such as SV40 large tumor antigen helicase (our positive control) are, therefore, able to act on their own, without the need for partners to activate their function.

The three-dimensional structure of RuvBL1 reveals an ADP molecule tightly bound between DI and DIII and that access to the ATPase active site is additionally blocked by hexamerization, thereby making the exchange between ADP and ATP impossible. Additional cofactors are, therefore, likely to be needed to open the nucleotide pocket. Proteins such as TIP60, c-Myc, and β-catenin have been shown to interact with RuvBL1 (3, 7, 14) and might be required by RuvBL1 to drive the conformational changes that would enable its function. A simpler example is given by bacterial RuvB, which by itself has weak ATPase and helicase activities *in vitro* and yet requires RuvA as a partner for its *in vitro* and *in vivo* activities (61). It may, therefore, be impossible to clearly detect ATPase and helicase activity in RuvBL1 unless a functional complex is reconstituted with additional accessory proteins. A similar problem has already been reported for many histone acetylases; most cannot efficiently acetylate histones within chromatin contexts *in vitro* when using the purified recombinant protein (62, 63). For this reason it has been proposed that additional cofactors are required for acetylation of the relevant substrates.

The hexameric ring-shaped structure of RuvBL1, the nucleic acid binding studies, and the fact that RuvBL1 is an AAA$^+$ protein suggest that it could act as a molecular motor protein. Given that RuvBL1 is part of several important complexes, we conclude that it has to work together with other proteins present in the cell for proper function. The understanding of how RuvBL1 function is regulated by the different steps of ATP hydrolysis and by interacting proteins will deepen our understanding of the central role RuvBL1 plays in the essential processes of life.

Acknowledgments—We thank Dr. Bernard Haendler for helpful suggestions during the preparation of this manuscript, Dr. Roman Hillig for advice on how to design the domain II constructs, and Dr. Vera Pütter for help in establishing the helicase assay.

REFERENCES

1. Bauer, A., Huber, O., and Kemler, R. (1998) *Proc. Natl. Acad. Sci. U. S. A.* **95,** 14787–14792
2. Shen, X., Mizuguchi, G., Hamiche, A., and Wu, C. (2000) *Nature* **406,** 541–544
3. Ikura, T., Ogryzko, V. V., Grigoriev, M., Groisman, R., Wang, J., Horikoshi, M., Scully, R., Qin, J., and Nakatani, Y. (2000) *Cell* **102,** 463–473
4. Kanemaki, M., Makino, Y., Yoshida, T., Kishimoto, T., Koga, A., Yamamoto, K., Yamamoto, M., Moncollin, V., Egly, J. M., Muramatsu, M., and Tamura, T. (1997) *Biochem. Biophys. Res. Commun.* **235,** 64–68
5. Jonsson, Z. O., Dhar, S. K., Narlikar, G. J., Auty, R., Wagle, N., Pellman, D., Pratt, R. E., Kingston, R., and Dutta, A. (2001) *J. Biol. Chem.* **276,** 16279–16288
6. Qiu, X. B., Lin, Y. L., Thome, K. C., Pian, P., Schlegel, B. P., Weremowicz, S., Parvin, J. D., and Dutta, A. (1998) *J. Biol. Chem.* **273,** 27786–27793
7. Bauer, A., Chauvet, S., Huber, O., Usseglio, F., Rothbacher, U., Aragnol, D., Kemler, R., and Pradel, J. (2000) *EMBO J.* **19,** 6121–6130
8. Jonsson, Z. O., Jha, S., Wohlschlegel, J. A., and Dutta, A. (2004) *Mol. Cell* **16,** 465–477
9. Fuchs, M., Gerber, J., Drapkin, R., Sif, S., Ikura, T., Ogryzko, V., Lane, W. S., Nakatani, Y., and Livingston, D. M. (2001) *Cell* **106,** 297–307
10. Teixeira, M. T., Dujon, B., and Fabre, E. (2002) *J. Mol. Biol.* **321,** 551–561
11. Khorasanizadeh, S. (2004) *Cell* **116,** 259–272
12. Stein, G. S., Zaidi, S. K., Braastad, C. D., Montecino, M., van Wijnen, A. J., Choi, J. Y., Stein, J. L., Lian, J. B., and Javed, A. (2003) *Trends Cell Biol.* **13,** 584–592
13. Kusch, T., Florens, L., Macdonald, W. H., Swanson, S. K., Glaser, R. L., Yates, J. R., III, Abmayr, S. M., Washburn, M. P., and Workman, J. L. (2004) *Science* **306,** 2084–2087
14. Wood, M. A., McMahon, S. B., and Cole, M. D. (2000) *Mol. Cell* **5,** 321–330
15. Dugan, K. A., Wood, M. A., and Cole, M. D. (2002) *Oncogene* **21,** 5835–5843
16. Feng, Y., Lee, N., and Fearon, E. R. (2003) *Cancer Res.* **63,** 8726–8734
17. Newman, D. R., Kuhn, J. F., Shanab, G. M., and Maxwell, E. S. (2000) *RNA*

6, 861–879
18. King, T. H., Decatur, W. A., Bertrand, E., Maxwell, E. S., and Fournier, M. J. (2001) *Mol. Cell. Biol.* **21,** 7731–7746
19. Gartner, W., Rossbacher, J., Zierhut, B., Daneva, T., Base, W., Weissel, M., Waldhausl, W., Pasternack, M. S., and Wagner, L. (2003) *Cell Motil. Cytoskeleton* **56,** 79–93
20. Neuwald, A. F., Aravind, L., Spouge, J. L., and Koonin, E. V. (1999) *Genome Res.* **9,** 27–43
21. Gorbalenya, A. E., Koonin, E. V., Donchenko, A. P., and Blinov, V. M. (1989) *Nucleic Acids Res.* **17,** 4713–4730
22. Schmid, S. R., and Linder, P. (1992) *Mol. Microbiol.* **6,** 283–291
23. Patel, S., and Latterich, M. (1998) *Trends Cell Biol.* **8,** 65–71
24. Putnam, C. D., Clancy, S. B., Tsuruta, H., Gonzalez, S., Wetmur, J. G., and Tainer, J. A. (2001) *J. Mol. Biol.* **311,** 297–310
25. Yamada, K., Kunishima, N., Mayanagi, K., Ohnishi, T., Nishino, T., Iwasaki, H., Shinagawa, H., and Morikawa, K. (2001) *Proc. Natl. Acad. Sci. U. S. A.* **98,** 1442–1447
26. Tsaneva, I. R., Muller, B., and West, S. C. (1993) *Proc. Natl. Acad. Sci. U. S. A.* **90,** 1315–1319
27. Gorynia, S., Matias, P. M., Gonçalves, S., Coelho, R., Thomaz, M., Haendler, B., Donner, P., and Carrondo, M. A. (2006) *Acta Crystallogr. Sect. F* **62,** 61–66
28. Kabsch, W. (1993) *J. Appl. Crystallogr.* **26,** 795–800
29. Collaborative Computational Project Number 4 (1994) *Acta Crystallogr. Sect. D* **50,** 760–763
30. Jones, T. A., Zou, J. Y., Cowan, S. W., and Kjeldgaard, M. (1991) *Acta Crystallogr. Sect A* **47,** 110–119
31. Roussel, A., Fontecilla-Camps, J. C., and Cambillau, C. (1990) in *XV IUCr Congress Abstracts*, pp. 66–67, International Union of Crystallography Bordeaux, France
32. Murshudov, G. N., Vagin, A. A., and Dodson, E. J. (1997) *Acta Crystallogr. Sect. D* **53,** 240–255
33. Schomaker, V., and Trueblood, K. N. (1968) *Acta Crystallogr. Sect. B* **24,** 63–76
34. Lamzin, V. S., and Wilson, K. S. (1993) *Acta Crystallogr. Sect. D* **49,** 129–147
35. Laskowski, R. A., MacArthur, M. W., Moss, D. S., and Thornton, J. M. (1993) *J. Appl. Crystallogr.* **26,** 283–291
36. Ramachandran, G. N., and Sasisekharan, V. (1968) *Adv. Prot. Chem.* **23,** 283–438
37. Berman, H. M., Westbrook, J., Feng, Z., Gilliland, G., Bhat, T. N., Weissig, H., Shindyalov, I. N., and Bourne, P. E. (2000) *Nucleic Acids Res.* **28,** 235–242
38. Lenzen, C. U., Steinmann, D., Whiteheart, S. W., and Weis, W. I. (1998) *Cell* **94,** 525–536
39. Li, D., Zhao, R., Lilyestrom, W., Gai, D., Zhang, R., DeCaprio, J. A., Fanning, E., Jochimiak, A., Szakonyi, G., and Chen, X. S. (2003) *Nature* **423,** 512–518
40. Gai, D., Zhao, R., Li, D., Finkielstein, C. V., and Chen, X. S. (2004) *Cell* **119,** 47–60
41. Enemark, E. J., and Joshua-Tor, L. (2006) *Nature* **442,** 270–275
42. Rappas, M., Schumacher, J., Niwa, H., Buck, M., and Zhang, X. (2006) *J. Mol. Biol.* **357,** 481–492
43. Mancini, E. J., Kainov, D. E., Grimes, J. M., Tuma, R., Bamford, D. H., and Stuart, D. I. (2004) *Cell* **118,** 743–755
44. Holm, L., and Sander, C. (1993) *J. Mol. Biol.* **233,** 123–138
45. Bochkarev, A., Pfuetzner, R. A., Edwards, A. M., and Frappier, L. (1997) *Nature* **385,** 176–181
46. Sullivan, C. S., and Pipas, J. M. (2002) *Microbiol. Mol. Biol. Rev.* **66,** 179–202
47. Borowiec, J. A., Dean, F. B., Bullock, P. A., and Hurwitz, J. (1990) *Cell* **60,** 181–184
48. Niedenzu, T., Roleke, D., Bains, G., Scherzinger, E., and Saenger, W. (2001) *J. Mol. Biol.* **306,** 479–487
49. Singleton, M. R., Sawaya, M. R., Ellenberger, T., and Wigley, D. B. (2000) *Cell* **101,** 589–600
50. Fletcher, R. J., Bishop, B. E., Leon, R. P., Sclafani, R. A., Ogata, C. M., and Chen, X. S. (2003) *Nat. Struct. Biol.* **10,** 160–167
51. Ahnert, P., and Patel, S. S. (1997) *J. Biol. Chem.* **272,** 32267–32273
52. Kaplan, D. L., and Steitz, T. A. (1999) *J. Biol. Chem.* **274,** 6889–6897
53. Yu, X., Hingorani, M. M., Patel, S. S., and Egelman, E. H. (1996) *Nat. Struct. Biol.* **3,** 740–743
54. Makino, Y., Kanemaki, M., Kurokawa, Y., Koji, T., and Tamura, T. (1999) *J. Biol. Chem.* **274,** 15329–15335
55. Carlson, M. L., Wilson, E. T., and Prescott, S. M. (2003) *Mol. Cancer* **2,** 42
56. Watkins, N. J., Lemm, I., Ingelfinger, D., Schneider, C., Hossbach, M., Urlaub, H., and Luhrmann, R. (2004) *Mol. Cell* **16,** 789–798
57. Allen, G. C., Jr., and Kornberg, A. (1991) *J. Biol. Chem.* **266,** 22096–22101
58. Ayora, S., Stasiak, A., and Alonso, J. C. (1999) *J. Mol. Biol.* **288,** 71–85
59. Tarumi, K., and Yonesaki, T. (1995) *J. Biol. Chem.* **270,** 2614–2619
60. Ustav, M., Ustav, E., Szymanski, P., and Stenlund, A. (1991) *EMBO J.* **10,** 4321–4329
61. Friedberg, E. C., Walker, G. C., Siede, W., Wood, R. D., Schultz, R. A., and Ellenberger, T. (2005) *DNA Repair and Mutagenesis*, 2nd Ed., pp. 569–613, American Society for Microbiology, Washington, D. C.
62. Grant, P. A., Schieltz, D., Pray-Grant, M. G., Steger, D. J., Reese, J. C., Yates, J. R., III, and Workman, J. L. (1998) *Cell* **94,** 45–53
63. Ogryzko, V. V., Kotani, T., Zhang, X., Schiltz, R. L., Howard, T., Yang, X. J., Howard, B. H., Qin, J., and Nakatani, Y. (1998) *Cell* **94,** 35–44
64. Wallace, A. C., Laskowski, R. A., and Thornton, J. M. (1995) *Protein Eng.* **8,** 127–134
65. Sanner, M. F., Olson, A. J., and Spehner, J. C. (1996) *Biopolymers* **38,** 305–320
66. Hubbard, S. J., and Thornton, J. M. (1993) *NACCESS*, Department of Biochemistry and Molecular Biology, University College, London
67. McDonald, I. K., and Thornton, J. M. (1994) *J. Mol. Biol.* **238,** 777–793